Janusz KALISZ[1*]
Wit GRZESIK[2]
Krzysztof ZAK[2]
Kazimierz CZECHOWSKI[1]

PROPERTIES OF THE SUBSURFACE LAYER AFTER ROLLING BURNISHING OF AN INITIALLY MILLED ALUMINIUM ALLOY

This paper characterizes mechanical properties of the technological subsurface layer produced by medium milling of EM AW-AlCu4MgSi(A) aluminium alloy in hardened state T451 using a ball-end cutter and subsequent roller burnishing using a nitride ceramic ball. It was revealed that ball burnishing operations performed on curvilinear milled surfaces allow obtaining the subsurface layer with a minimum strain-hardening effect and induced compressive residual stresses without visible microstructural changes. As a result, such functional properties of the subsurface layer as fatigue strength, bearing properties and contact strength along with a very smooth machined surface of the *Sa* roughness of about 0.02 μm can be ensured.

1. INTRODUCTION

Nowadays, a growing group of lightweight alloys such as aluminium, magnesium and titanium alloys finds wider applications in many industry sectors (aircraft, automotive, precision, mechanical engineering) [1,2] In particular, aluminium alloys represent a good machinability in comparison to steels which promotes their manufacturing using HSM technique and recently also hybrid machining processes [3]. It is observed that the advanced industry sectors apply more and more hybrid/sequential machining technologies which are more efficient, sustainable and generate lower production costs. They can be based on the combination of removal and non-removal machining operations, i.e. subsequent turning or milling and burnishing operations. As a result, it is a very competitive alternative for typical finishing cutting and abrasive operations [4,5]. One of the predominant advantages is that these sequential processes can be performed on CNC lathes or multi-axis CNC machining centers with commercial cutting and burnishing tools [4,6,7]. Roller and sliding burnishing improve distinctly the surface integrity including

_____
[1] Institute of Advanced Manufacturing Technology, Krakow, Poland
[2] Opole University of Technology, Faculty of Mechanical Engineering, Poland
  E-mail: janusz.kalisz@ios.krakow.pl

surface topography, strain-hardening index and the distribution and profile of the residual stresses [8,9]. Another important fact is that burnishing can be effective for both hard and soft ferrous and non-ferrous materials, including plastics. These positive technological and mechanical effects were positively examined for several aluminium alloys such as aluminium 6061 [9,10], AA 6463E [11], 2014 [12] and EM AW-AlCu4MgSi(A [7] grades. The effects can be magnified by using multi-pass burnishing technology [11]. Burnishing tools can be stored in the tool magazine of a CNC lathe or machining centre and both medium and finish operations can be performed at one working stand which contributes to the reduction of the machining cost and time [6,7]. In this paper the results of measurements of strain–hardening effect and residual stresses induced in the subsurface layer after the ball burnishing of concave and convex mould parts made of a EM AW-AlCu4MgSi(A) aluminium alloy of 110 HB hardness are presented. In addition, microstructural changes beneath the subsurface layer were examined using SEM technique and EDS analysis. The characterization of the surface topography produced for the same workpiece material and under the same machining conditions was presented in Ref. [7].

2. EXPERIMENTAL DETAILS

2.1. CHARACTERIZATION OF WORKPIECE AND EXPERIMENTAL METHODOLOGY

In this study the workpiece material used was a EN AW-AlCu4MgSi(A) aluminium alloy in the hardened state T451 of the quality guaranteed by the metallurgical certificate 3.1. This alloy features high tensile strength of UTS=445 MPa and the yield stress Y=292 MPa. In addition, it has a good corrosion resistance but a low weldability. Apart from its main applications in aircraft industry, manufacturing industry, weapon (armaments) and automotive industry, it is used in mould industry due to the necessity of final polishing (it can be optionally replaced by finish burnishing). Tables 1 and 2 specify its chemical composition and the mechanical properties [7].

Table 1. Chemical composition of EN AW-AlCu4MgSi(A) alloy

Al	Ti	Si	Fe	Cu	Mn	Mg	Cr	Zn	Ti+Zr	others
91.3-95.5	0.06	0.64	0.04	4.2	0.95	0.76	0.04	0.17	0.06	0.02

Table 2. Mechanical properties of EN AW-AlCu4MgSi(A) alloy

Ultimate tensile strength UTS [MPa]	Yield stress Y [MPa]	Elongation A5 [%]	Hardness [HB]	Density [g/cm^3]
445	292	17	110	2.80

The concave specimens with the curvature radius of 250 mm and the dimensions of a 80 mm in width and a 120 mm in length were initially milled using a monolithic ball-end cutter (VHM) of a 8 mm diameter with the cutting speed of v_c = 350 m/min, the feed per tooth of f_z = 0.04 mm, the pitch (stepover) of f_{wf} =0.53 mm and the axial depth of cut a_p = 0.5 mm. Milling operation (Fig. 1b) was performed with the constant stepover and the tilt angle ψ= 7.5° in the direction perpendicular to the Y axis (Fig. 1b).

Both milling and burnishing operations were carried out using a 5-axis machining centre model DMC 75V Linear as shown in Fig. 1a. Burnishing operations were performed using a spring-loaded burnishing tool equipped with a Si_3N_4 ceramic polished ball of a 8 mm diameter. The offset of the burnishing tool was equal to 0.3 mm by appropriate spring deflection (see burnishing tool as a detail in Fig. 1a). The working feed of the table was the same at f_t = 6000 mm/min for all burnishing trials. The value of the spring load was equal to F_n = 75 N and the feed rate in the direction perpendicular to milling lays (Fig. 1c) was equal to f_{wn}=0.02 mm. Similar process kinematics was applied in Ref. [6]. During burnishing the ball was lubricated by machine oil. All CNC programs used are edited using a NX CAM programming system.
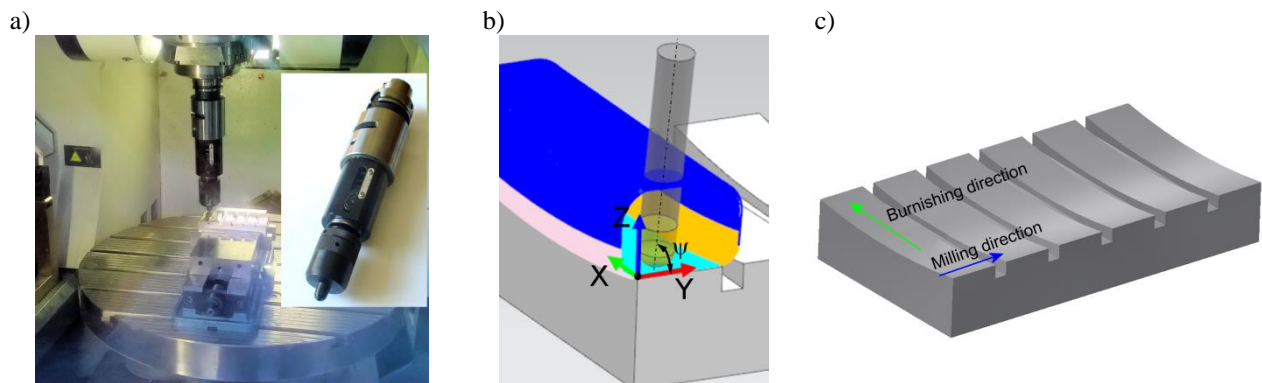

Fig. 1. The view of the working space of machining center and burnishing tool (a), visualization of ball-end milling in the direction perpendicular to the Y axis (b), the specimen with marked directions of working movements (c) [7]

2.2. MEASUREMENTS OF MICRO-HARDNESS

Measurements of micro-hardness distribution across the subsurface layer were performed using a Vickers hardness tester model LECO MHT Series 200 under the load of 0.25 N (25 G), i.e. micro-hardness $HV_{0.025}$ was measured. All indentation tests were performed on the sections inclined at 5-6° to the outer surface. The sections were prepared by grinding, mechanical and vibration polishing. This method allows minimizing the effects of interfaces of neighbouring indentations and increasing the measuring accuracy. The first indentation was done at the distance of 15 μm from the surface and next ones keeping the distance of 5 μm. The distance between measuring lines was equal to 350 μm. The dimensions and details of the specimens with inclined sections on both concave and convex surfaces are presented in Fig. 2. The average hardness of the bulk material was equal to 137 $HV_{0,025}$. The changes of micro-hardness along the cross-section of the subsurface

layer were assessed by means of the strain-hardening ratio. This ratio S_h was determined from the following equation:

$$S_h = \frac{HV_{max} - HV_b}{HV_b} 100\%$$
(1)

where: HV_b – hardness of the bulk material, HV_{max} – maximum hardness measured.
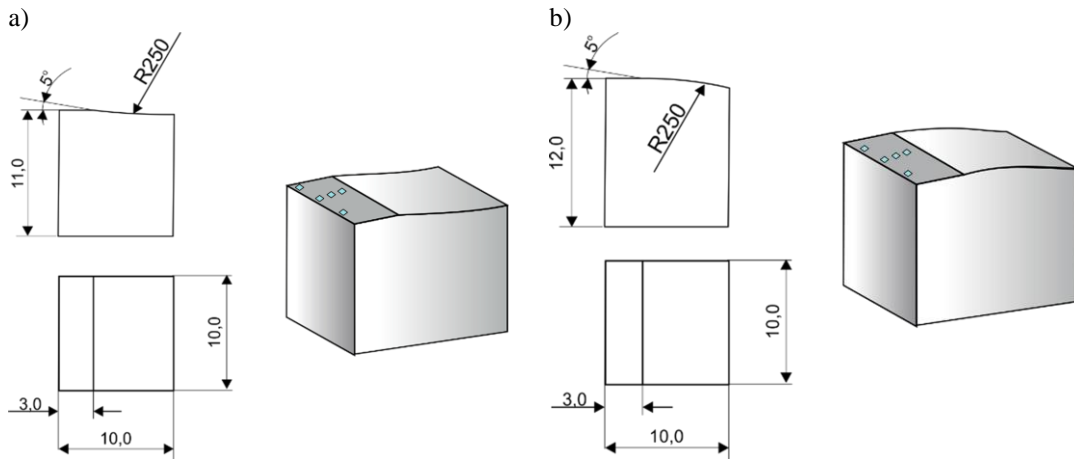

Fig. 2. Inclined sections for micro-hardness tests on concave: a) convex, b) surfaces

2.3. MEASUREMENTS OF RESIDUAL STRESSES

Measurements of the residual stresses induced by hybrid ball-end milling and roller burnishing operations were carried out using the XRD technique and two methods (the classical sin2ψ and g-sin2ψ methods). In general, XRD macroscopic residual stress measurements provide the arithmetic average stress in a diffracting volume defined by he size of the irradiated area and the depth of penetration of the X-ray beam [13,14].
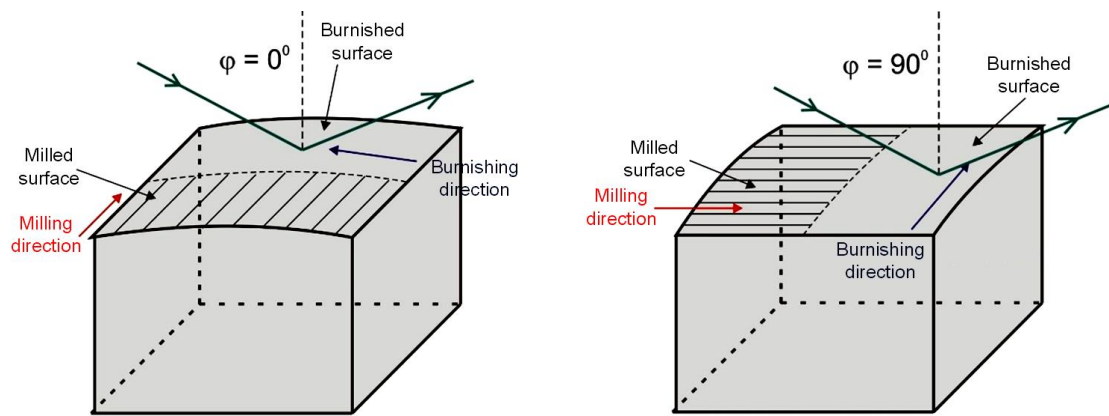

Fig. 3. Direction of X-ray beam in relation to burnishing direction: a) parallel with $\varphi=0°$
and b) perpendicular with $\varphi=90°$

The magnitude of the residual stress was determined keeping Young's modulus E=70.14 GPa and Poisson's ratio ν=0.35 for the main Al phase in the aluminium alloy used. Fig. 3 presents the orientation of X-ray beam in relation to the direction of the machined lays. It is the same for concave and convex specimens. As a result, residual stresses can be measured in the direction parallel σ_{xx} (Fig. 3a) and perpendicular σ_{yy} (Fig. 3b) to the burnishing lays. The residual stress (RS) measurements were performed using X'Pert PRO, PANanalytical X-ray diffractometer equipped with a cooper anode lamp (Cuλ $K\alpha$ = 1.5406 Å) and 5-axis table. In addition, the relevant measurements by means of g-sin2ψ method were carried out using a Siemens D500 diffractometer using the same anode lamp and identical specimens shown in Fig. 3.

3. EXPERIMENTAL RESULTS AND DISCUSSION

The effects of the ball burnishing of initially milled surfaces based on the characterization of the mechanical features of the subsurface layer are presented in Figs. 4-8. Figs. 4 and 5 present the distribution of micro-hardness beneath the subsurface layer and the strain hardening effect respectively.
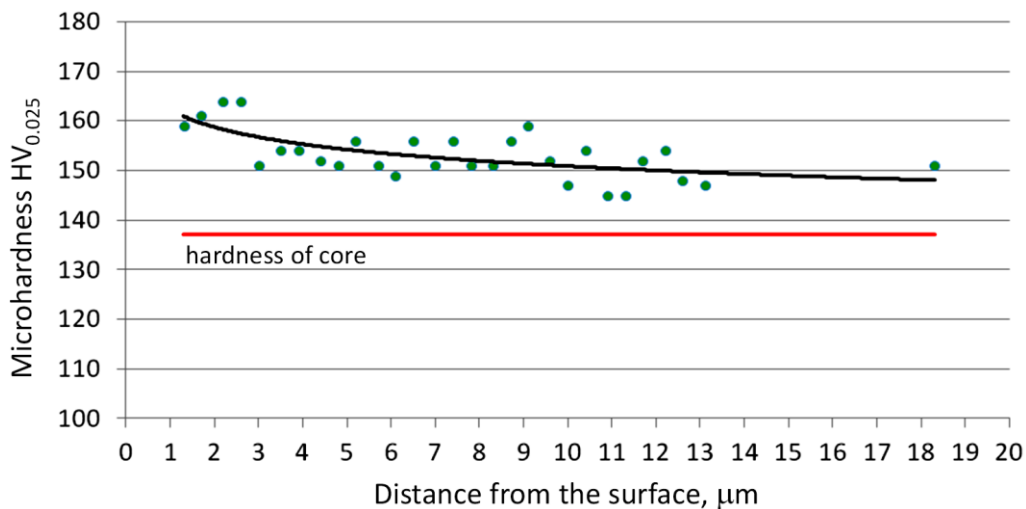

Fig. 4. Changes of micro-hardness $HV_{0,025}$ from the concave surface for burnishing load F_n = 75 N and feed f_{wn} = 0.02 mm

As shown in Fig. 4 the maximum micro-hardness of about 160 $HV_{0,025}$. was determined close to the surface at a very small distance of 1-2 µm and the strain hardening effect is induced at about 20 µm beneath the surface. It should be noticed that similar burnishing effects occur for both concave and convex surfaces. On the other hand, the maximum values of strain hardening ratio are equal to 20% and 17% for concave and convex surfaces respectively. The low values of strain hardening ratio indicate that the burnishing covers preliminarily the asperities and strain hardening penetrate only to about 20 µm (effectively to about 10 µm) beneath the surface.
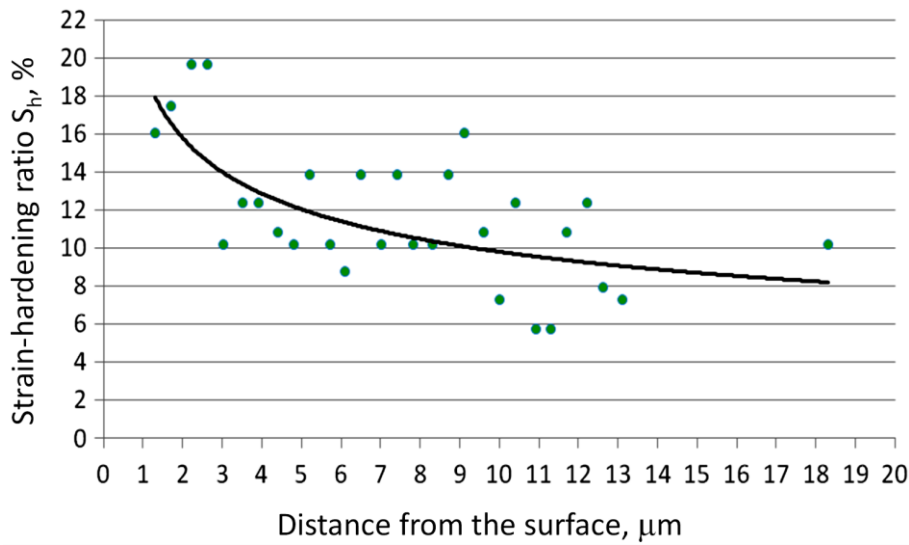
Fig. 5. Changes of strain-hardening ratio from the concave surface for burnishing load $F_n = 75$ N
and feed $f_{wn} = 0.02$ mm

Fig. 6 shows that the RS value depends on the measurement direction and the shape of burnished surface. In the direction parallel to the machined lays the tensile stresses of about 50 MPa are produced on concave specimens and the compressive stresses of about -230 MPa on convex specimens. On the other hand, in the direction perpendicular to the machined lays the compressive stresses of about -350 MPa and about -150 MPa are produced on concave and convex specimens respectively. The maximum residual stresses of about -350 MPa occur after burnishing of convex surfaces. It should be noted that the sign of residual stresses induced by ball-end milling is rather of random nature.
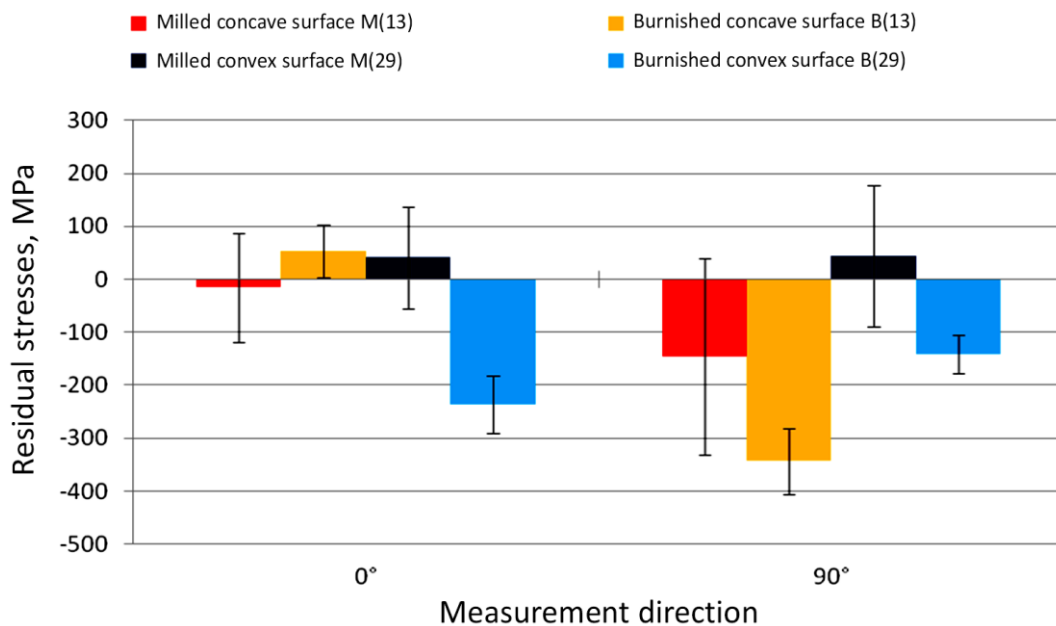

Fig. 6. Comparison of residual stresses acting in directions parallel (σ_{xx}) and perpendicular (σ_{yy}) to burnishing lays for concave and convex specimens ($F_n = 75$ N, $f_{wn} = 0.02$ mm)
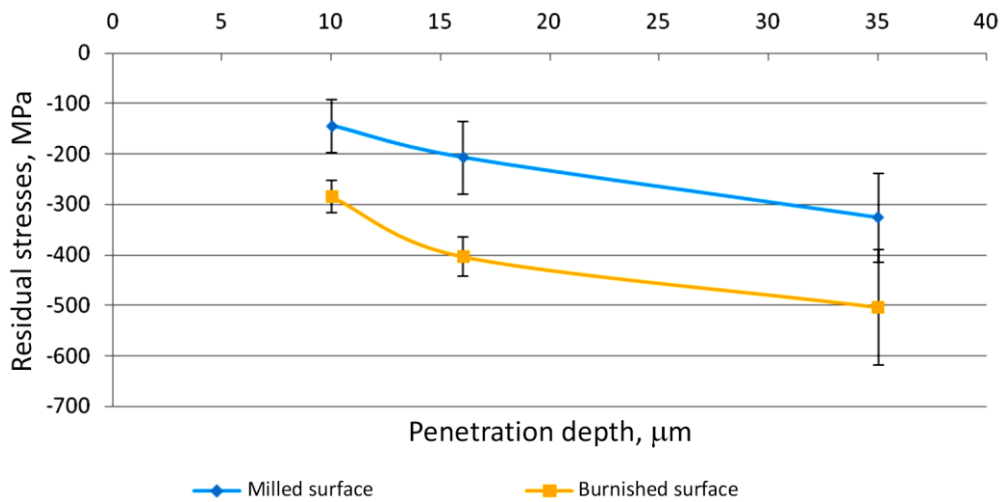
Fig. 7. The dependence of RS distribution on the penetration depth of X-ray beam for a concave specimen No. 13
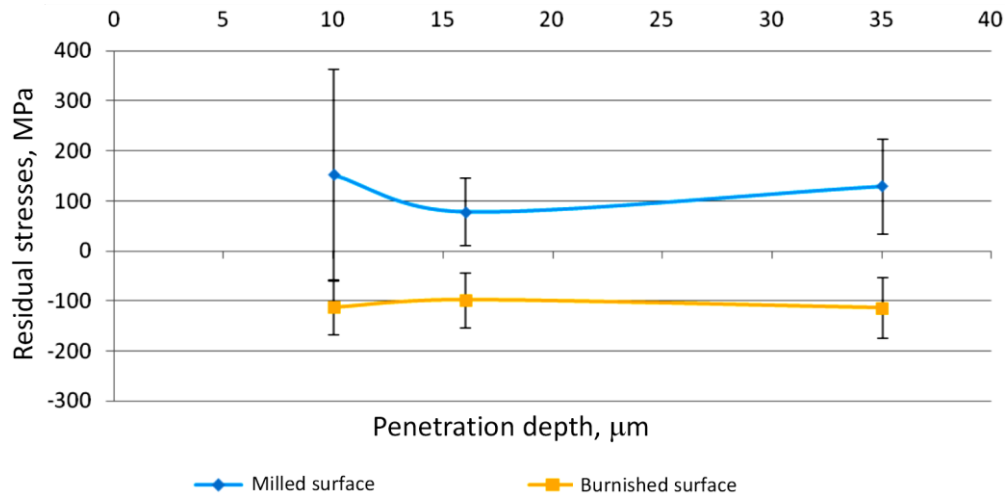($F_n = 75$ N, $f_{wn} = 0.02$ mm)

Fig. 8. The dependence of RS distribution on the penetration of X-ray beam for a convex specimen No. 29
($F_n = 75$ N, $f_{wn} = 0.02$ mm)

Fig. 7 and 8 present the RS distributions obtained by means of a g-sin2ψ method based on the depth of X-ray beam penetration. It allows determining the RS at the depth of about 10 μm and deeper beneath the machined surface. It should be noted that for a concave surface residual stresses are compressive after ball-end milling as well as after roller burnishing. Consequently, the final RSs are about -350 MPa whereas for the convex surface the final RSs are also compressive but distinctly lower at -100 MPa. This difference results from the fact that ball-end milling induces tensile RSs at above 100 MPa.

Analysis of micro-structures within the subsurface layer was performed using SEM technique. A scanning electron microscope model JEOL JSM-6460LV equipped with EDS analyzer was employed. Exemplarily, Fig. 9 compares SEM images of subsurface layers obtained for the magnification 5000× and both concave (Fig. 9a) and convex (Fig. 9b) burnished surfaces.
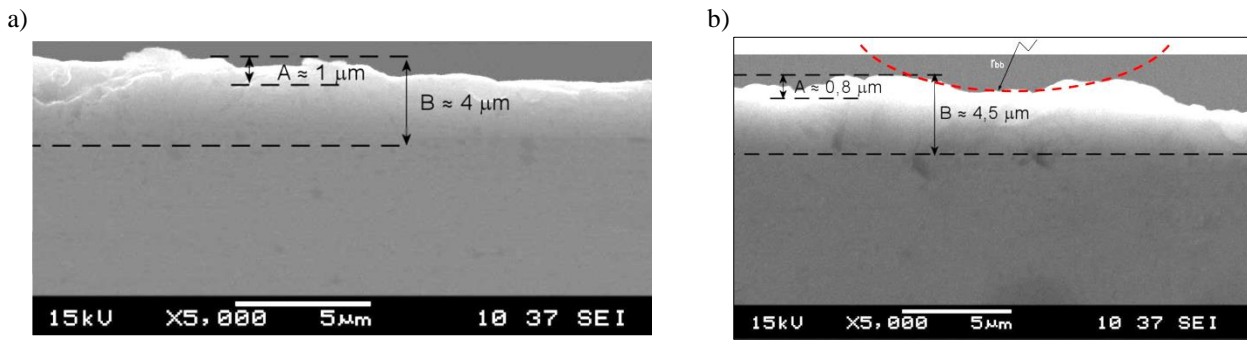
a)

b)

Fig. 9. SEM images of subsurface layers obtained for concave (a) and convex (b) burnished surfaces;
(A-surface profile, B- subsurface layer)

It can be observed in Fig. 9 that cold plastic deformation of surface irregularities penetrates at the distance 4-4.5 µm and this observation corresponds satisfactorily with the earlier distribution of strain-hardening effect (S-HE) presented in Fig. 5. In fact, the visible changes of the S-HE are localized near the surface at the depth of about 5 µm below. At this high magnification the deformation of surface irregularities resulting from the copying of the burnishing ball can be easily recognized.
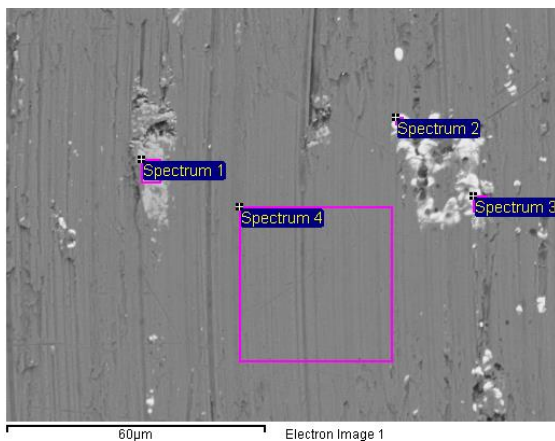
Spectrum	O	Mg	Al	Si	Mn	Fe	Cu	All
1	1.5	0.3	52.4	5.8	14.0	17.8	8.2	100.0
2	0.8	0.3	40.4	0.3	-	-	58.2	100.0
3	1.2	0.5	48.5	0.3	-	-	49.5	100.0
4	1.2	0.8	92.6	0.5	-	-	4.8	100.0

Fig. 10. EDS analysis of subsurface layer obtained for a convex burnished surface
($F_n = 75$ N, $f_{wn} = 0.02$ mm)

Fig. 10 presents the result of EDS analysis performed for the subsurface layer of a convex burnished specimen in four selected points denoted by appropriate labels *Spectrum 1-4*. The EDS results specified in the table confirm that after burnishing no phase transformation occur.

4. CONCLUSIONS

1. An aluminium alloy is slightly deformed during ball burnishing operations and, as a result, the burnished surfaces are smoothed and optical quality sculptured surfaces

are produced [1]. Moreover, burnishing causes that the subsurface layer is moderately strain-hardened and, in general, compressive residual stresses are induced.

2. The strain-hardening index is equal to 17%-20% when both concave and convex parts made of an aluminium alloy are burnished with the normal load of 75 N and a small feed of 0.02 mm. In fact, the depth of an effective strain hardening is about 10 μm. This superficial effect is comparable to polishing.

3. The compressive residual stresses are induced into the subsurface layer under burnishing conditions selected in this study. This is due to fact that plastic deformations are not intensive and are rather localized in the areas of surface asperities. The maximum value of residual compressive stress measured near the concave surface was equal to -300 MPa which coincides well with other literature data [9].

4. Micro-structural changes do not practically occur in the subsurface layer at the micro scale but can be observed at nano-scale which requires more advanced technique such as TEM.

5. It can be reasoned that hybrid processes including ball-end milling and ball burnishing seem to be highly efficient in improving surface quality of complex aluminium parts and producing the subsurface layer with good mechanical and functional properties.

REFERENCES

[1]   OCZOS K., KAWALEC A., 2011, *Manufacturing of lightweight constructions*, PWN, Warsaw, (in Polish).

[2]   SIENIAWSKI J., 2009, *Aluminium alloys applied in aircraft manufacturing*, Mechanik, 7, 649-654, (in Polish).

[3]   GRZESIK W., 2017, *Advanced machining processes of metallic materials,* Elsevier Amsterdam.

[4]   GRZESIK W., ŻAK K., PRAŻMOWSKI M., 2012, *Surface integrity of hard turned parts modified by ball burnishing,* J. Mach. Eng. 12, 18-27.

[5]   GRZESIK W., RECH J., ŻAK K., 2015, *Characterization of surface textures generated on hardened steel parts in high-precision machining operations*, Int. J. Adv. Manuf. Technol., 1-8.

[6]   GROCHAŁA D., BERCZYŃSKI S., GRZĄDZIEL Z., 2015, *Stress in the surface layer of objects burnished after milling,* Int. J. Adv. Manuf. Technol. 72, 1655-1663.

[7]   KALISZ J., ŻAK K., GRZESIK W., CZECHOWSKI K., 2015, *Characteristics of surface topography after roller burnishing of EM AW-AlCu4MgSi(A) aluminium alloy*, J. Mach. Eng., 15/1, 71-80.

[8]   PRZYBYLSKI W., 1987, *Technology of burnishing*, WNT, Warsaw, (in Polish).

[9]   EL-AXIR M.H., 2007, *An investigation into the ball burnishing of aluminium alloy 6061-T6,* Proc. IMechE, Part B: J. Engineering Manufacture, 221, 1733-1742.

[10] EL-TAYEB N.S.M., LOW K.O., BREVERN P.V, 2007, *Influence of roller burnishing contact width and burnishing orientation on surface quality and tribological behaviour of Aluminium 6061*, J. Mater. Proc. Technol. 186, 272-278.

[11] NEMAT M., LYONS A.C., 2000, *An investigation of the surface topography of ball burnished mild steel and aluminium,* Int. J. Adv. Manuf. Technol., 16, 469-473.

[12] EL-AXIR M.H., OTHMAN O.M., ABODIENA A.M., 2008, *Improvements in out-of-roundness and microhardness of inner surfaces by internal ball burnishing process,* J. Mater. Proc. Technol. 196, 120-128.

[13] PREVEY P.S., 1986, *X-ray diffraction residual stress techniques,* Metals Handbook, 10, Metals Park, American Society for Metals.

[14] GRZESIK W., ŻAK K., 2014, *Characterization of surface integrity produced by sequential dry hard turning and ball burnishing operations*, J. Manuf. Sci, Technol. 136, 031017-1-031017-9.